Acta Materialia 107 (2016) 213–219

Contents lists available at ScienceDirect

Acta Materialia

journal homepage: www.elsevier.com/locate/actamat

Full length article

Revealing the relationships between chemistry, topology and stiffness of ultrastrong Co-based metallic glass thin films: A combinatorial approach

Volker Schnabel [a, *], Mathias Köhler [b], Simon Evertz [a], Jana Gamcova [c, d], Jozef Bednarcik [c], Denis Music [a], Dierk Raabe [b], Jochen M. Schneider [a]

[a] Materials Chemistry, RWTH Aachen University, Kopernikusstr. 10, D-52074 Aachen, Germany
[b] Max-Planck-Institut für Eisenforschung, Max-Planck-Straße 1, D-40237 Düsseldorf, Germany
[c] Deutsches Elektronen Synchrotron DESY, FS-PE Group, Notkestrasse 85, D-22607 Hamburg, Germany
[d] Pavol Jozef Šafárik University, Department of Condensed Matter Physics, Park Angelinum 9, Košice, Slovakia

ARTICLE INFO

Article history:
Received 16 October 2015
Received in revised form
25 January 2016
Accepted 25 January 2016
Available online xxx

Keywords:
Metallic glass
Topology
Combinatorics
Hybridization

ABSTRACT

An efficient way to study the relationship between chemical composition and mechanical properties of thin films is to utilize the combinatorial approach, where spatially resolved mechanical property measurements are conducted along a concentration gradient. However, for thin film glasses many properties including the mechanical response are affected by chemical topology. Here a novel method is introduced which enables spatially resolved short range order analysis along concentration gradients of combinatorially synthesized metallic glass thin films. For this purpose a CoZrTaB metallic glass film of 3 μm thickness is deposited on a polyimide foil, which is investigated by high energy X-ray diffraction in transmission mode. Through the correlative chemistry-topology-stiffness investigation, we observe that an increase in metalloid concentration from 26.4 to 32.7 at% and the associated formation of localized (hybridized) metal – metalloid bonds induce a 10% increase in stiffness. Concomitantly, along the same composition gradient, a metalloid-concentration-induced increase in first order metal - metal bond distances of 1% is observed, which infers itinerant (metallic) bond weakening. Hence, the metalloid concentration induced increase in hybridized bonding dominates the corresponding weakening of metallic bonds.

1. Introduction and motivation

Chemistry-topology-property relationships of metallic glasses have been a topic of intense discussion [1–5]. Metallic glasses fall into two groups, namely those with [6] and those without metalloids [7]. The most common synthesis techniques for metallic glasses are bulk casting [8–10] and melt spinning [11]. In these studies, chemical composition is varied through multiple synthesis experiments. By employing conventional bulk synthesis techniques, metallic glasses are developed as a result of multiple, sequential bulk synthesis experiments, often based on trial-and-error approaches [1,2,12–15]. In contrast, combinatorial thin film synthesis has been used to systematically study the chemistry-topology-property relationship of various materials systems [16,17]. Recently, combinatorial metallic glass synthesis by physical vapor deposition has been employed to study the chemistry – mechanical property relationship of metallic glass thin films [18]. Furthermore, literature has shown clear agreement between bulk and thin film properties of Co-based metal-metalloid metallic glasses regarding elasticity, density and magnetism [19,20]. Ergo, combinatorial thin film synthesis can be an efficient tool to investigate the chemistry-topology-property relationship of metallic glasses in general. However, up to now there is no high throughput method present in literature to study the chemically induced topological evolution along a defined compositional gradient of metallic glass thin films [18]. The short range order of metallic glasses is usually studied by sequential synthesis of homogeneous specimen and analysis employing high energy diffraction experiments [1,5,19,20], which is an inefficient way of investigating the chemistry-topology-mechanical properties relationship.

* Corresponding author.
E-mail address: schnabel@mch.rwth-aachen.de (V. Schnabel).

http://dx.doi.org/10.1016/j.actamat.2016.01.060
1359-6454/

The topology of metallic glasses without metalloids is strongly determined by dense packing [7,21], whereas the topology of metal-metalloid metallic glasses is additionally influenced by strong covalent bonding [5,6,19,22]. Due to the complex chemistry-topology-property relationships the design of metal-metalloid metallic glasses is challenging [6,13,23]. The metal-metalloid Co-based metallic glasses discussed here possess a unique local atomic configuration [5,22,24], which leads to the combination of extraordinary high fracture strength of above 5000 MPa and high Young's modulus of 268 GPa [13]. It is inferred in the literature that through chemically induced topology changes, properties such as glass formability [1,3,6], magnetic properties [2] and mechanical properties [3,4,19,25] can be enhanced. The Young's modulus [19,22] as well as the elastic limit [5] have also been reported to exhibit a strong topological dependence. In the case of Co-based metallic glasses it has been observed that the metal-metalloid short range order is strongly affecting the mechanical properties [5,19,20,22]. Furthermore, it has been reported for Fe–Cr–Mo–P–C–B metallic glasses that an increase in metalloid concentration increases the number of strongly bound metal-metalloid clusters, which on the other hand weakens the metal-to-metal bonds [26]. These chemical-induced topology changes have implications on how shear stress may be accommodated [26]. Hence, an influence on the Young's modulus, shear modulus and plasticity of these type of metal-metalloid metallic glasses has been observed [6]. The discussion above suggests that understanding the chemistry-topology-property relationship is an essential prerequisite to the knowledge-based design of strong metallic glasses.

The objective of this work is to describe the chemically induced topology and stiffness changes of Co–Zr–Ta–B metallic glass thin films. A novel method is introduced, where the chemically induced topology and stiffness changes are measured along a composition gradient of Co–Zr–Ta–B metallic glass thin films. For this purpose a combinatorial metal-metalloid Co–Zr–Ta–B metallic glass thin film is deposited by physical vapor deposition [19,27] on low X-ray scattering and radiation damage tolerant thin polyimide foil [28]. The topological analysis of the combinatorial thin film is performed in transmission, using high energy X-ray diffraction [29].

2. Experimental procedure

Combinatorial Co–Zr–Ta–B metallic glass thin films were magnetron sputtered onto Si and polyimide substrates. The film deposited onto the 50.8 mm Si (100) substrate was used for chemical and mechanical characterization, while the films on 50 μm thick radiation damage tolerant polyimide foil [28] were employed for structural analysis. The base pressure of the system was $6 \cdot 10^{-5}$ Pa [30]. The films were synthesized from circular elemental targets with a diameter of 50 mm and a purity of 99.95% for Co, Zr and Ta and 99.5% for B. The applied power densities were 2.0, 1.6, 0.3 and 8.4 W/cm^2 for Co, Zr, Ta and B targets, respectively. The three metals were sputtered using separate direct current (DC) power supplies, whereas B was sputtered with a radio frequency power supply. As a sputtering gas Ar with a pressure of 0.4 Pa was employed. The targets were tilted by 19° normal to the substrate as described in Fig. 1 and the target to substrate distance was 10 cm. The deposition time was 3 h resulting in a film thickness of 3 μm.

The chemical composition was analyzed by three dimensional atom probe tomography (3D-APT). The APT samples were prepared according to a standard lift-out procedure [31] using focused-ion-beam (FIB) cutting. The measurements were performed in a commercial local electrode atom probe (LEAP 3000X HR, CAMECA Instruments) in voltage mode.

The APT result was used for a standard calibration of the energy dispersive X-ray analysis (EDX). The chemical composition was measured along the concentration gradients as indicated in Fig. 1. A spacing between the individual measuring points of 4 mm was chosen, corresponding to a gradient of 0.2 at% B per mm along the Ta–B gradient.

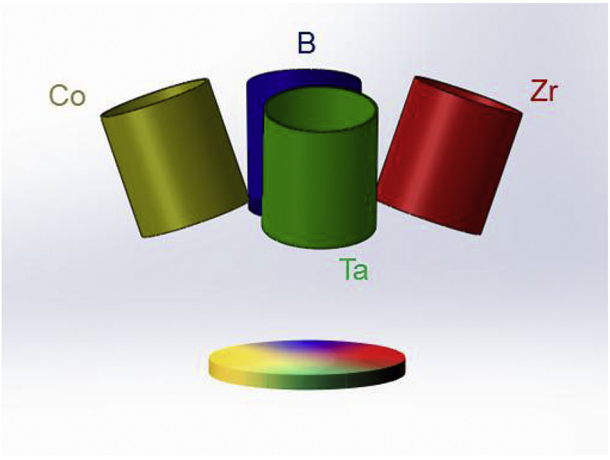

Fig. 1. Schematic drawing of the combinatorial deposition setup. The chemical symbols denote the direction of the elemental sputtering sources, which results in the schematic compositional gradient depicted. The measurements were performed along the B – Ta and the Co – Zr gradient with a spacing of 4 mm between the individual measurement points.

The topology analysis was performed by applying high energy X-ray diffraction at the P02.1 beamline of the PETRA III electron storage ring at DESY (Hamburg, Germany). A monochromatic photon beam with a wavelength of $\lambda = 0.02071$ nm and a beam size of 0.7 mm × 0.7 mm was used. The diffraction was recorded in transmission using the thin film sample deposited on polyimide foil. Each measuring point was illuminated for 30 s and the diffracted photons were recorded as 2D patterns with a fast image plate detector Perkin Elmer 1621. The sample to detector distance was set to be 246 mm, whereas the q vector ($q = 4\pi \sin\theta/\lambda$) up to 14 Å^{-1} was used [29].

The 2D diffraction patterns were integrated into q-space using the FIT2D software package [32]. The background was directly subtracted from the 2D diffraction patterns. The data sets were corrected for polarization, sample absorption, fluorescence contribution and inelastic scattering using the PDFgetX2 software [33]. The total structural factor was obtained from the normalized elastically scattered intensity according to the Faber-Ziman equation [34]. The pair distribution functions (PDFs) were obtained by a sine Fourier transform using standard procedure described elsewhere [12,19].

After chemical and structural analysis, the reduced Young's modulus was measured along the concentration gradient using a depth-sensing nanoindenter (Hysitron TriboIndenterTM). A Berkovich indenter with a tip radius of 100 nm was used. A maximum indentation load of 1000 μN was employed, which corresponded to a contact depth of less than 10% of the film thickness. 24 indentations were performed for each film composition. The Oliver and Pharr method [30] was applied to extract the reduced Young's modulus.

3. Results and discussion

3.1. Chemical analysis

Due to the geometrical arrangement of the magnetrons with respect to the substrate normal (Fig. 1) and the chosen 10 cm target

to substrate distance, the deposition of the chemically graded thin films is achieved. The Co content obtained by the combinatorial deposition ranges from 31.9 to 45.5 at %, the Zr content from 26.1 to 34.4 at %, the B content from 26.4 to 32.7 at %, and the Ta content from 1.0 to 2.6 at %. The magnitude of the composition gradients are a consequence of the power supplied to the magnetrons and the difference in sputter yield of the elements [35].

3.2. Short range order analysis

Four representative pair distribution functions obtained from measurements along the B–Ta concentration gradient are presented in Fig. 2 in a range of 2–4 Å. The PDFs are presented with an equally spaced offset in vertical direction for better comparison purposes. The dashed lines in Fig. 2 represent the total PDFs, whereas the solid and dotted graphs represent Gaussian deconvolutions of two individual bond population distributions. It can be observed that for all compositions the first order coordination shell is split into two separate bond distance populations. The chemical composition corresponding to the individual PDFs are presented next to the graphs. For the composition with the lowest B content at the bottom, the solid and dotted vertical lines indicate the maxima, (2.61 and 3.01 Å), of the first and second bond population, respectively. As observed in Fig. 2, both maxima shift continuously to higher distances with increasing B content from bottom to top. Peak positions of the first and second maxima for the highest B content are at 2.63 and 3.05 Å, (respectively), which yields a chemically induced change in relative bond distance of more than 1%. The error by deconvolution on the measured bond population maxima is below 0.1% in relative bond distance. By correlation with literature data on the CoZrTaB metallic glass system [24], where the bond distance derived from the atomic radii for a Co–Co first order bond length is 2.5 Å and the Zr–Zr first order bond distance is reported to be 3.2 Å, it is inferred that the first bond population (see Fig. 3) corresponds to Co–Co first order bonding, whereas the

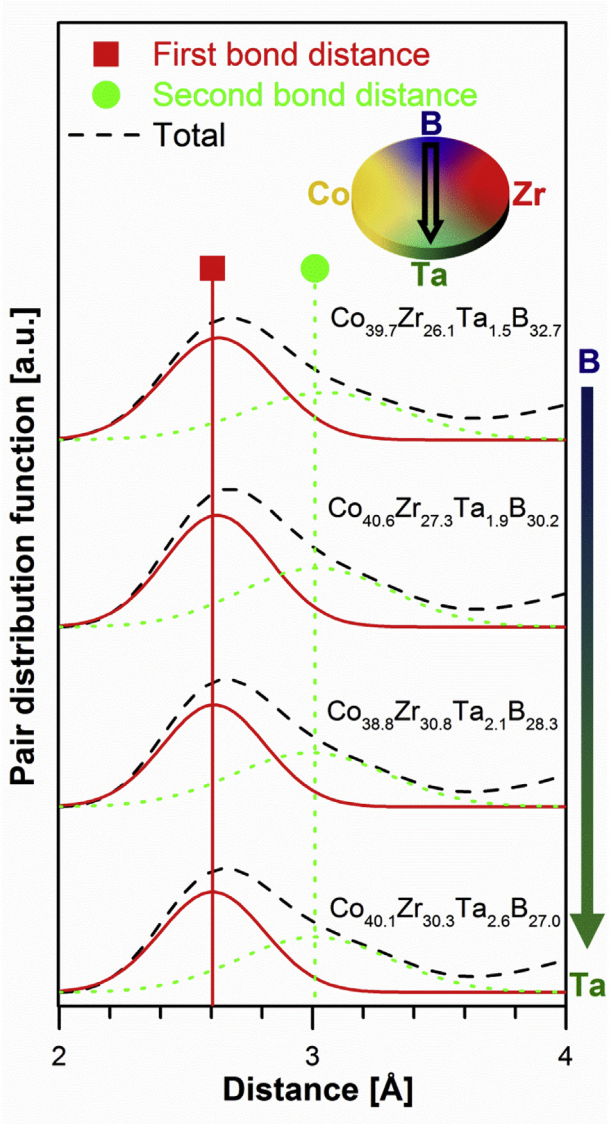

Fig. 2. Pair distribution functions with increasing B-content from bottom to top obtained by high energy X-ray diffraction are presented in a range between 2 and 4 Å. Next to the total pair distribution functions, the first and second bond population distributions are included, which are obtained by Gaussian peak deconvolution.

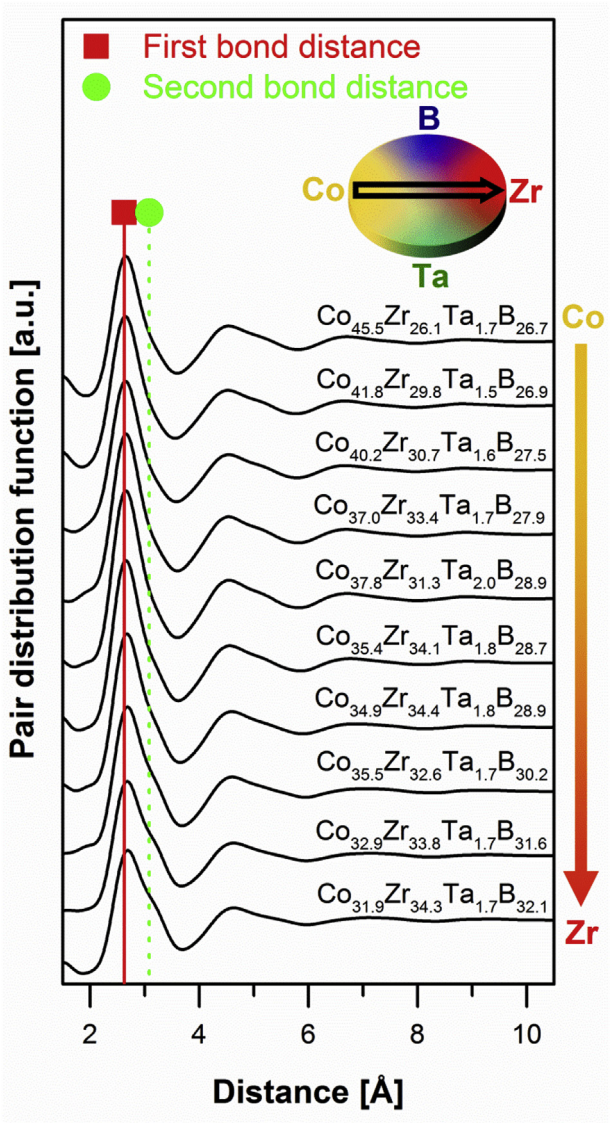

Fig. 3. The pair distribution functions with increasing Co content from bottom to top obtained by high energy X-ray diffraction are presented in a range from 1.5 to 10.5 Å. The data at the bottom were obtained for the highest Zr content, whereas the data at the top were acquired for the highest Co content. The peak with the maximum amplitude represents the first order coordination shell.

second bond population is dominated by Zr–Zr bonding. As expected, no prior peak around 2 Å is measured [5,19]. Hence, no metal to B and B to B bonds are visible in the measured PDFs. This can be attributed to the larger weighting factor of the metals compared to B [24,36]. Therefore, no direct structural information on the B topology can be obtained experimentally. However, the B content induced changes in metal-to-metal topology are directly accessible by scattering experiments. As previously mentioned, the first order Co–Co and Zr–Zr bond populations shift to higher bond distances as the B content is increased. An increasing bond distance causes bond weakening [37]. Thus, the here reported B-induced structural evolution validates the *ab initio* investigations by Gu et al. [6], predicting a metalloid-content-induced metal-to-metal bond weakening.

The PDFs obtained along the Co–Zr concentration gradient are investigated next to evaluate the metallic content-induced topological evolution. The PDFs with increasing Co content from bottom to top obtained by high energy X-ray diffraction are presented in a range between 1.5 and 10.5 Å in Fig. 3. The PDF at the bottom is obtained for the highest Zr content, whereas the PDF at the top is obtained for the highest Co content. The first peak at around 2.6 Å corresponds to the first order coordination shell, while the second, located between 3.7 and 6.0 Å, corresponds to the second order coordination shell. It is observed that a shoulder to the right of the first coordination shell peak appears as the Zr content is increased. This shoulder can be attributed to the Zr–Zr dominated bond population, which is consistent with the increase in Zr concentration along the Co–Zr gradient. In addition to the increase in bond population, a shift towards higher bond distances of about 3% is observed (see Fig. 3). Hence, it can be inferred that an increasing Zr content leads to a large population of Zr–Zr bonds. In order to further evaluate the topological splitting of the first coordination shell peak into Co–Co and Zr–Zr bond populations, spatially resolved chemical analysis is performed by APT.

Fig. 4a–c and Fig. 4d–f presents APT data of the CoZrTaB thin film from the center and from the edge of the B–Ta compositional gradient with average B-contents of 29.6 and 27.0 at%, respectively. The studies presented in Fig. 4 reflect the results of all five atom probe studies conducted at these two positions. Here the two data sets with the highest number of collected ions are presented with 8 and 8.5 million counts, respectively. APT images are presented in Fig. 4 part a) and d), where the spatially resolved chemical concentration profiles along the cylinders are presented in part b) and e), respectively. The APT measurements are conducted along the film growth direction. Iso-surfaces with the concentrations of 50.0 at% for Co and 28.3 at% for Zr are displayed in the APT images. It can be observed that nanoscale Co and Zr-rich phases are formed. The maximum compositional difference between these two phases is about 15 at% for Co (see Fig. 4b), which is higher compared to the compositional gradient of the average Co content. Fig. 4c indicates that the measured (open circles) and the ideal (lines) distributions do not correspond. The p-value shows the probability of obtaining the observed reduced χ^2 with a confidence level of 99%. The p-values <0.0001 for both APT measurements for all four elements strongly imply the non-randomness of the measured ion distributions. This separation in Co and Zr rich phases is consistent with the observed separation of the Co–Co and Zr–Zr bond population induced by an increase in Zr content. Hence, the notion regarding the presence of amorphous Co rich and Zr rich phases, which is suggested based on the topology analysis, is also supported by the spatially resolved chemical analysis. In contrast to the micrometer sized phase separation observed in bulk metallic glasses [38,39], the composition modulation observed here exhibits a periodicity of 20–30 nm perpendicular to the film growth direction. Chemical modulations are observed in all APT datasets obtained. The chemical distribution observed suggests that the high quenching rates [40] present in physical vapor deposition retard diffusion and consequently impede the evolution of long range order, as well as composition modulations, on length scales larger than the a few nm [38,39]. Nevertheless, the presence of chemical modulation on the nm scale may be explained by limited surface diffusion, (on the nm scale), enabled by the interaction of the energetic sputtered flux with the growing film surface [41]. Therefore, it is inferred that the combination of high quenching rates and limited ad-atom mobility enables the evolution of composition modulations on the nm length scale. Spinodal decomposition may induce nm scale chemical fluctuations in rapidly quenched bulk metallic glasses as reported for NiNbY [42] and ZrGdCoAl [43] systems. Furthermore, it is reported that these bulk metallic glasses exhibit a temperature induced increase in chemical modulations' amplitude, whereas the wavelength is unchanged [42,43]. This is also expected for the CoZrTaB system studied here. To evaluate the chemistry – topology – stiffness relationship, the chemically induced topology changes will next be correlated to the reduced Young's moduli obtained by nanoindentation.

3.3. Chemistry – topology – stiffness relationship

For the evaluation of the chemistry – topology – stiffness relationship the topological and reduced Young's moduli are depicted along the Co–Zr and B–Ta concentration gradients in Fig. 5. In the center of Fig. 5, the position of the first and second maxima of the metal-to-metal bond distance population is presented to the left and to the right, respectively. The distance of the first bond population maxima ranges from 2.61 to 2.63 Å. The distance of the second bond population maxima ranges from 2.99 to 3.08 Å, which is a variation of 3% in relative bond distance. For the second bond population maxima, the error by deconvolution is below 1%.

At the bottom of Fig. 5 the reduced Young's modulus and the schematic deposition setup are depicted to the left and right, respectively. The reduced Young's modulus varies between 183 and 203 GPa. Applying a Poisson's ratio of 0.28 [19] to the reduced Young's moduli obtained by nanoindentation, Young's moduli in the range of 201–227 GPa are obtained, which is smaller compared to 268 GPa reported for the CoFeTaB system [13]. Due to the smooth surface of the metallic glass thin film, the standard deviations of the stiffness measurements are between 3 and 6 GPa for each set of the 24 indentation measurements per composition. Thus, the observed increase in stiffness is statistically significant. The same conclusion can be drawn from Fig. 6 where the reduced Young's modulus measured along the B–Ta concentration gradient is presented as a function of B content including the error bars for the individual sets of stiffness measurements. The composition modulation discussed in section 3.2 exhibits a periodicity between 20 and 30 nm and is hence at least an order of magnitude lower than the indentation induced elastic stain field [44]. Despite the presence of composition modulations on the 10's of nm scale the elastic behavior appears to be primarily governed by the change in B-concentration within the combinatorial composition gradient. Furthermore, the hardness increase measured along the compositional gradient corresponds to the previously discussed increase in stiffness: As the B content is increased from 26.4 to 32.7 at% in our CoZrTaB metallic glass, the measured hardness values change from 12.0 to 13.7 GPa. The magnitude is comparable to Vickers hardness values of 15.4–15.9 GPareported for ternary bulk $Co_{58}Ta_7B_{35}$ and $Co_{56}Ta_9B_{35}$ metallic glasses, respectively [45]. The ternary bulk CoTaB metallic glasses are reported to exhibit a Young's modulus of 240–247 GPa, which is higher compared to the 201–227 GPa observed here. For the $Co_{54}Ta_{11}B_{35}$ bulk metallic glass with even higher Ta content a

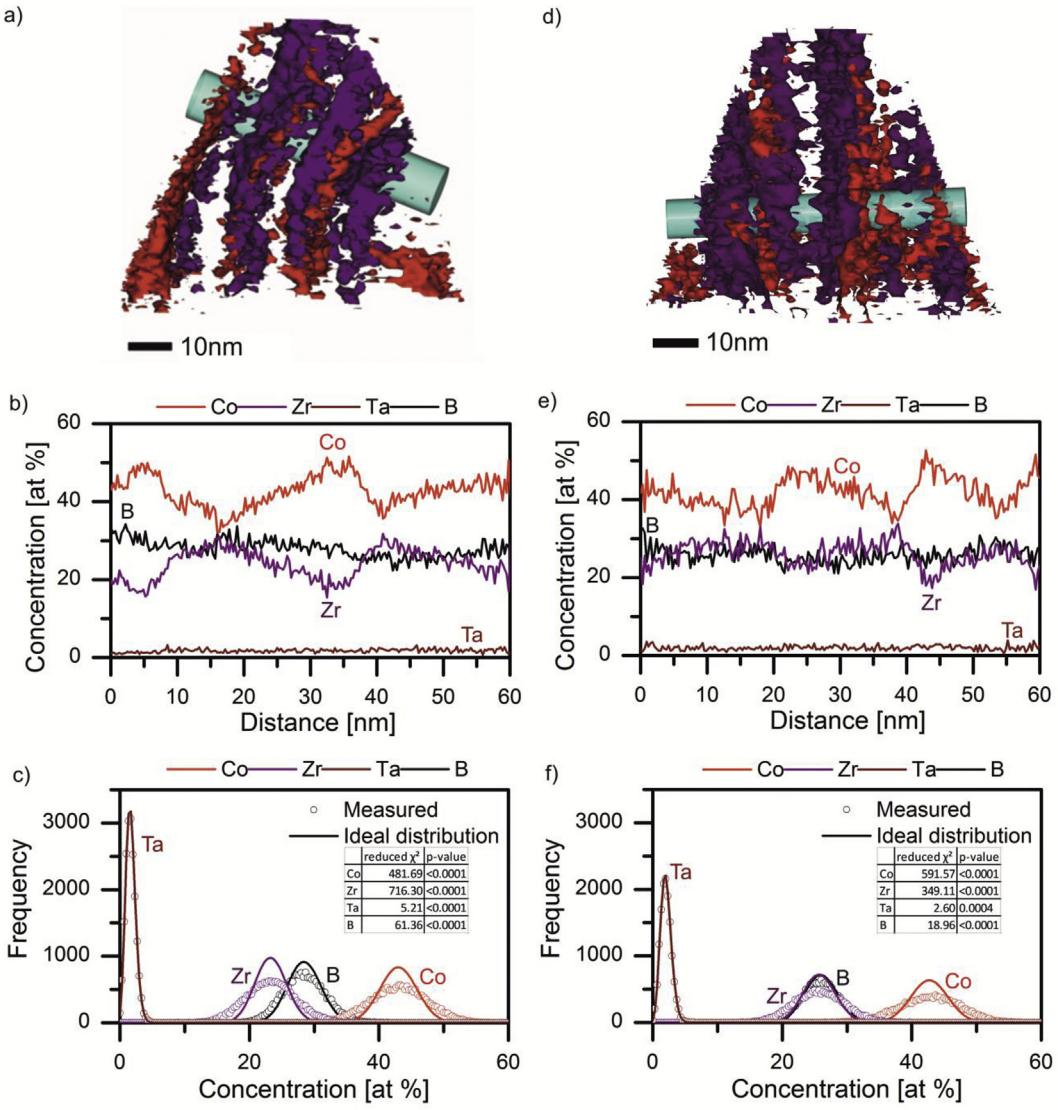

Fig. 4. a), d) Atom probe tomography images of the CoZrTaB metallic glass are presented including the iso-concentration surfaces of 50.0 at% for Co and 28.3 at% for Zr. The APT measurements are conducted along the film growth direction. Along the cylinder from left to right the concentration profile for Co, Zr, Ta and B are obtained and provided in b) and e), respectively. c), f) Frequency distribution functions are presented for the data obtained in a) and d), respectively. The inset table show the deviation between the ideal (lines) and the measured (open circles) distribution, such that the p-values indicate a non-random chemical distribution [47].

Vickers hardness of 17.1 GPa is reported [22]. It is proposed that both, the higher Young's modulus as well as the higher hardness reported in literature may be due to differences in composition.

It is observed from the reduced Young's modulus data in Fig. 5 that the stiffness increases almost continuously along both, the Ta to B and the Co to Zr concentration gradients. Along these concentration gradients the bond distances of Co–Co and Zr–Zr increase. Hence, the shortest Co–Co and Zr–Zr bond distances correspond to regions with the lowest Young's modulus, which is contradictory to the notion that shorter bond distances or in other words denser metal-to-metal packing causes an increase in bond stiffness [37]. For metallic glasses not containing metalloids it has been reported that denser packing leads to an increase in stiffness [46]. However, for the here studied metal – metalloid Co–Zr–Ta–B metallic glass thin film the metalloid concentration dominates stiffness. This observation is in agreement to the observations made by Wang et al. [22] and Hostert et al. [19], who propose strong, hybridized metal-B bonds to cause high stiffness of Co-based metallic glasses. It is reasonable to assume that with an increasing B content from 26.4 to 32.7 at% the fraction of hybridized metal-to-metalloid bonds increases, which is in line with the here measured stiffness data.

4. Conclusions

A novel method to effectively study the chemistry - topology - stiffness relationship of combinatorial thin film metallic glasses was introduced. The thin films are deposited on a radiation damage tolerant polyimide foil to enable high energy X-ray diffraction in transmission mode. EDX and APT were used to characterize chemical information along the concentration gradient, while the elastic properties were measured by nanoindentation. Through the correlative composition and stiffness analysis it is observed that the CoZrTaB glass exhibits an increase in stiffness by 10%, which is induced by an increase in B content from 26.4 to 32.7 at%. From the topology analysis along the same chemical gradient, it is understood that as the B content increases, the Co–Co and Zr–Zr first order bond distances increase by 1%, which implies weakening of

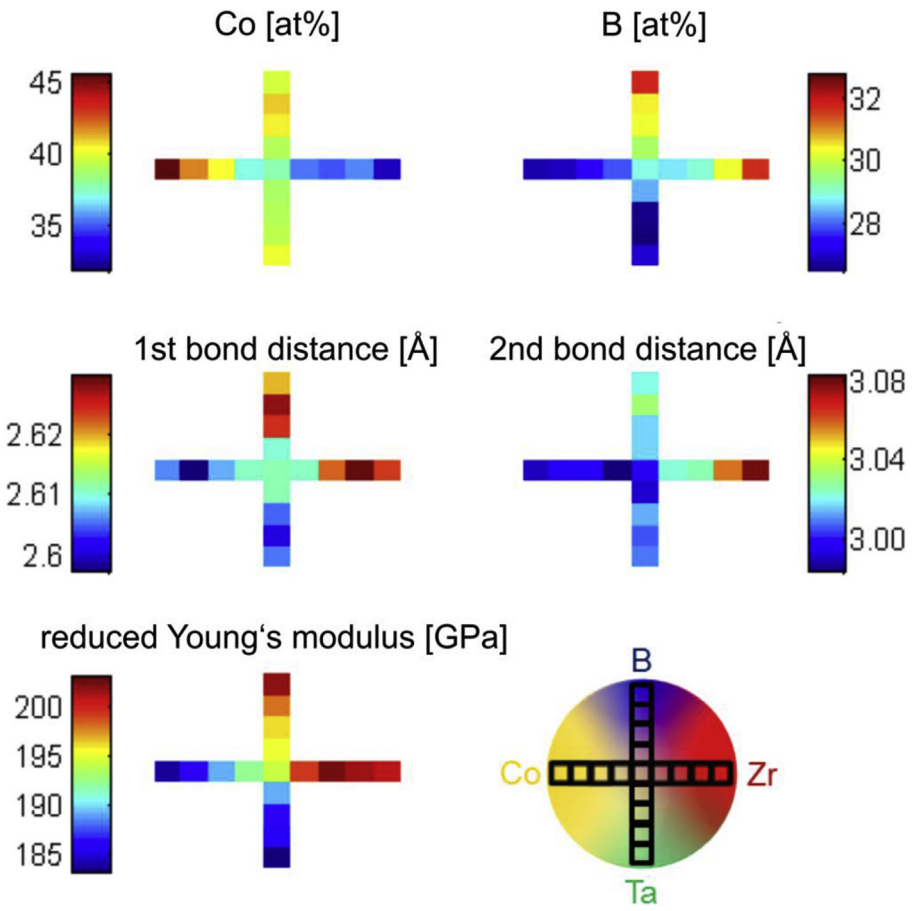

Fig. 5. The compositional, structural and stiffness measurements along the concentration gradients are depicted. At the top, the Co and B compositions are presented. In the center, maxima of the first and second metal-to-metal bond distance populations are given to the left and to the right, respectively. At the bottom, the reduced Young's modulus and the corresponding deposition schematic deposition is depicted to the left and right, respectively.

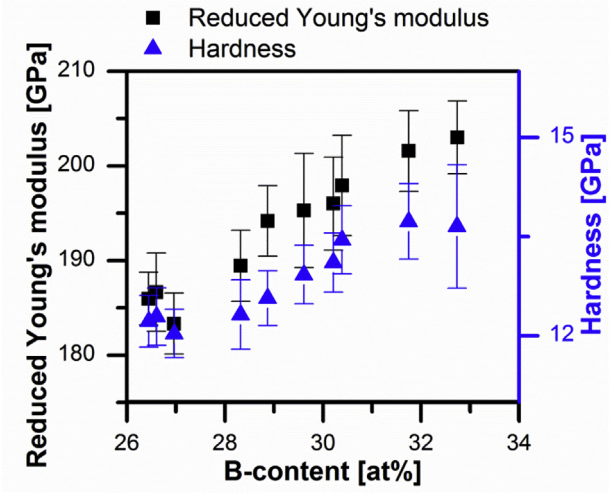

Fig. 6. The reduced Young's modulus and nanoindentation hardness are presented as a function of B-content. It is observed that with increasing B-content both the reduced Young's modulus and hardness increases.

bonds. This observation is consistent with *ab initio* studies [6] which predict a metalloid-concentration-induced metal bond weakening. Based on the correlative topology and stiffness analysis along the concentration gradients of a metallic glass thin film, it can be concluded that the B-content-induced increase in hybridization dominates the corresponding weakening of metallic bonds. Furthermore, a separation into amorphous nanoscale Co and Zr-rich phases is observed by both high energy X-ray diffraction and spatially resolved APT. It is proposed that the formation of composition modulations on the nm scale is due to the combination of ad-atom mobility, (limited to the nm length scale), and the high quenching rates associated with vapor phase condensation during magnetron sputtering.

Acknowledgments

This work was supported by the Deutsche Forschungsgemeinschaft within the SPP-1594 “Quantum mechanically guided design of ultra strong glasses”.

References

[1] A.H. Taghvaei, M. Stoica, M.S. Khoshkhoo, I. Kaban, J. Bednarcik, P. Jóvári, K. Janghorban, J. Eckert, DSC, XRD and TEM characterization of glassy $Co_{40}Fe_{22}Ta_8B_{30}$ alloy with very high thermal stabalility, Mater. Lett. 93 (2013) 322–325.
[2] I. Kaban, P. Jovari, A. Waske, M. Stoica, J. Bednarcik, B. Beuneu, N. Mattern, J. Eckert, Atomic structure and magnetic properties of Fe–Nb–B metallic glasses, J. Alloy. Compd. 586 (2014) 189–193.
[3] N. Chen, L. Martin, D.V. Luzguine-Luzgin, A. Inoue, Role Alloy. Addit. Glass Form. Prop. Bulk Metal. Glass. Mater. 3 (2010) 5320–5339.
[4] Q. Wang, C.T. Liu, Y. Yang, J.B. Liu, Y.D. Dong, J. Lu, The atomic-scale mechanism for the enhanced glass-forming-ability of a Cu-Zr based bulk metallic glass with minor element additions, Science 4 (2014) 4648.

[5] V. Schnabel, J. Bednarcik, D. Music, T. Pazur, C. Hostert, J.M. Schneider, Temperature-Induced Short-Range Order Changes in $Co_{67}B_{33}$ Glassy Thin Films and Elastic Limit Implications, Mater. Res. Lett. 3 (2015) 82–87.
[6] M.P. Moody, L.T. Stephenson, A.V. Ceguerra, S.P. Ringer, Quantitative Binomial Distribution Analyses of Nanoscale Like-Solute Atom Clustering and Segregation in Atom Probe Tomography Data, Microsc. Res. Tech. 71 (2008) 542–550.
[7] J. Ding, Y.-Q. Cheng, E. Ma, Full icosahedra dominate local order in $Cu_{64}Zr_{34}$ metallic glass and supercooled liquid, Acta Mater. 69 (2014) 343–354.
[8] E. Soinila, K. Antin, S. Bossuyt, H. Hänninen, Bulk metallic glass tube casting, J. Alloy. Compd. 509s (2011) S210–S213.
[9] K.J. Laws, G. Gun, M. Ferry, Effect of die-casting parameters on the production of high quality bulk metallic glass samples, Mater. Sci. Eng. A 425 (2006) 114–120.
[10] S. Wu, B. Shen, A. Inoue, Preparation and properties study of bulk $Fe_{75.5}Ga_3P_{10.5}C_4B_4Si_3$ metallic glass ring by copper mold casting, Intermetallics 12 (2004) 1261–1264.
[11] H.H. Liebermann, C.D. Graham, Production of amorphous alloy ribbons and effects of apparatus parameters on ribbon dimensions, Trans. Mag. 12 (1976) 921–923.
[12] A.H. Taghvaei, M. Stoica, J. Bednarcik, I. Kaban, H.S. Shahabi, M.S. Khoshkhoo, K. Janghorban, J. Eckert, Influence of ball milling on atomic structure and magnetic properties of $Co_{40}Fe_{22}Ta_8B_{30}$ glassy alloy, Mater. Charact. 92 (2014) 96–105.
[13] A. Inoue, B.L. Shen, H. Koshiba, H. Kato, A.R. Yavari, Ultra-high stength above 5000 MPa and soft magnetic properties of Co-Fe-Ta-B bulk glassy alloys, Acta Mater 52 (2004) 1631–1637.
[14] B. Shen, A. Inoue, Enhancement of the fracture strength and glass-forming ability of CoFeTaB bulk glassy alloy, J. Phys. Condens. Matter 17 (2005) 5647–5653.
[15] A. Inoue, B.L. Shen, C.T. Chang, Fe- and Co-based bulk glassy alloys with ultrahigh strength, Intermetallics 14 (2006).
[16] T. Gebhardt, D. Music, T. Takahashi, J.M. Schneider, Combinatorial thin film materials science: From alloy discovery and optimization to alloy design, Thin Solid Film. 520 (2012) 5491–5499.
[17] T. Gebhardt, D. Music, D. Kossmann, M. Ekholm, I.A. Abrikosov, L. Vitos, J.M. Schneider, Elastic properties of fcc Fe–Mn–X (X = Al, Si) alloys studied by theory and experiment, Acta Mater 59 (2011) 3145–3155.
[18] S. Ding, Y. Liu, Y. Li, Z. Liu, S. Sohn, F.J. Walker, J. Schroers, Combinatorial development of bulk metallic glasses, Nat. Mater 13 (2014) 494–500.
[19] C. Hostert, D. Music, J. Bednarcik, J. Keckes, V. Kapaklis, B. Hjörvarsson, J.M. Schneider, *Ab initio* molecular dynamics model for density, elastic properties and short range order of Co-Fe-Ta-B metallic glass thin films, J. Phys. Condens. Matter 23 (2011) 475401.
[20] C. Hostert, D. Music, V. Kapaklis, B. Hjörvarsson, J.M. Schneider, Density, elastic and magnetic properties of Co–Fe–Ta–Si metallic glasses by theory and experiment, Scr. Mater 66 (2012) 765–768.
[21] L. Zhang, Y. Cheng, A. Cao, J. Xu, E. Ma, Bulk metallic glasses with large plasticity: Composition design from the structural perspective, Acta Mater 57 (2009) 1154–1164.
[22] J. Wang, R. Li, R. Xiao, T. Xu, Y. Li, Z. Liu, L. Huang, N. Hua, G. Li, Y. Li, Y. Zhang, Compressibility and hardness of Co-based bulk metallic glass: A combined experimental and density functional theory study, Appl. Phys. Lett. 99 (2011) 151911.
[23] P.F. Guan, T. Fujita, A. Hirata, Y.H. Liu, M.W. Chen, Structural Origins of the Excellent Glass Forming Ability of $Pd_{40}Ni_{40}P_{20}$, Phys. Rev. Lett. 108 (2012) 175501.
[24] J. Bednarcik, K. Saksl, R. Nicula, S. Roth, H. Franz, Influence of cryomilling on structure of CoFeZrB alloy, J. Non-Cryst. Solid. 354 (2008) 5117–5119.
[25] W. Yang, H. Liu, Y. Zhao, A. Inoue, K. Jiang, J. Huo, H. Ling, Q. Li, B. Shen, Mechanical properties and structural features of novel Fe-based bulk metallic glasses with unprecedented plasticity, Sci. Rep. 4 (2014).
[26] X.J. Gu, J. Poon, G.J. Shiflet, M. Widom, Mechanical properties, glass transition temperature, and bond enthalpy trends of high metalloid Fe-based bulk metallic glasses, Appl. Phys. Lett. 92 (2008) 161910.
[27] Y. Liu, S. Hata, K. Wada, A. Shimokohbe, Thermal, mechanical and electrical properties of Pd-Based thin-film metallic glass, Jpn. J. Appl. Phys. 40 (2001) 5382–5388.
[28] J. Megusar, Low temperature fast-neutron and gamma irradiation of Kapton® polyimide films, J. Nucl. Mater. 245 (1997) 185–190.
[29] J. Bednarcik, S. Venkataraman, O. Khvostikova, H. Franz, D.J. Sordelet, J. Eckert, Microstructural changes induced by thermal treatment in $Cu_{47}Ti_{33}Zr_{11}Ni_8Si_1$ metallic glass, Mater. Sci. Eng. A 498 (2008) 335–340.
[30] W.C. Oliver, G.M. Pharr, An improved technique for determining hardness and elastic modulus using load displacement sensing indentation experiments, J. Mater. Res. 7 (1992) 1564–1583.
[31] K. Thompson, D. Lawrence, D.J. Larson, J.D. Olson, T.F. Kelly, B. Gorman, In situ site-specific specimen preparation for atom probe tomography, Ultramicroscopy 107 (2007) 131–139.
[32] A.P. Hammersley, S.O. Svensson, M. Hanfland, A.N. Fitch, D. Häusermann, Two-dimensional detector software: from real detector to idealised image or two-theta scan, High Press. Res. 14 (1995) 235–248.
[33] (a) X. Qiu, J.W. Thompson, S.J.L. Billinge, X. Qiu, J.W. Thompson, S.J.L. Billinge, PDFgetX2: a GUI-driven program to obtain the pair distribution function from X-ray powder diffraction data, J. Appl. Crystallogr. 37 (2004) 678–682;
(b) J. Appl. Cryst. 37 (2004) 678.
[34] T.E. Faber, J.M. Ziman, A theory of electrical properties of liquid metals, Philos. Mag. 11 (1965) 153–173.
[35] M.P. Seah, C.A. Clifford, F.M. Green, I.S. Gilmore, An accurate semi-empirical equation for sputtering yields I: for argon ions, Surf. Interface Anal. 37 (2005) 444–458.
[36] I. Kaban, P. Jovari, M. Stoica, J. Eckert, W. Hoyer, B. Beuneu, Topological and chemical ordering in $Co_{43}Fe_{20}Ta_{5.5}B_{31.5}$ metallic glass, Phys. Rev. B 79 (2009) 212201.
[37] M.L. Cohen, Calculation of bulk moduli of diamond and zinc-blende solids, Phys. Rev. B 32 (1985) 7988–7991.
[38] X.H. Du, J.C. Huang, H.M. Chen, H.S. Chou, Y.H. Lai, K.C. Hsieh, J.S.C. Jang, P.K. Liaw, Phase-separated microstructures and shear-banding behavior in a designed Zr-based glass-forming alloy, Intermetallics 17 (2009) 607–613.
[39] J. He, N. Mattern, J. Tan, J.Z. Zhao, I. Kaban, Z. Wang, L. Ratke, D.H. Kim, W.T. Kim, J. Eckert, A bridge from monotectic alloys to liquid-phase-separated bulk metallic glasses: Design, microstructure and phase evolution, Acta Mater. 61 (2013) 2102–2112.
[40] T.W. Barbee, W.H. Holmes, D.L. Keith, M.K. Pyzyna, Synthesis of amorphous niobium-nickel alloys by vapor quenching, Thin Solid Film. 45 (1977) 591–599.
[41] A. Abdulkadhim, M.T. Baden, V. Schnabel, M. Hans, N. Thieme, C. Polzer, P. Polcik, J.M. Schneider, Crystallization kinetics of V2AlC, Thin Solid Film. 520 (2012) 1930–1933.
[42] N. Mattern, G. Goerigk, U. Vainio, M.K. Miller, T. Gemming, J. Eckert, Spinodal decomposition of Ni-Nb-Y metallic glasses, Acta Mater. 57 (2009) 903–908.
[43] J.H. Han, N. Mattern, U. Vainio, A. Shariq, S.W. Sohn, D.H. Kim, J. Eckert. Phase separation in $Zr_{56-x}Gd_xCo_{28}Al_{16}$ metallic glasses ($0 < x < 20$). vol. 66. p.262–272.
[44] B.R. Lawn, M.V. Swain, Microfracture beneath point indentations in brittle solids, J. Mater. Sci. 10 (1975) 113–122.
[45] J. Wang, R. Li, N. Hua, T. Zhang, Co-based ternary bulk metallic glasses with ultrahigh strength and plasticity, J. Mater. Res. 26 (2011) 2072–2079.
[46] W.H. Wang, The elastic properties, elastic models and elastic perspectives of metallic glasses, Prog. Mater Sci. 57 (2012) 487–656.
[47] M.P. Moody, L.T. Stephenson, A.V. Ceguerra, S.P. Ringer, Quantitative binomial distribution analyses of nanoscale like-solute atom clustering and segregation in atom probe tomography data, Microsc. Res. Tech. 71 (2008) 542–550.